Engineering giant Rashba spin-orbit splitting in graphene via *n-p* codoping

Shifei Qi,[1,2,3] Yulei Han,[3,*] Fuming Xu,[4] Xiaohong Xu,[2,†] and Zhenhua Qiao[3,‡]

[1]*Department of Physics, Hebei Normal University, Shijiazhuang, Hebei 050024, China*

[2]*School of Chemistry and Materials Science, Shanxi Normal University, Linfen, Shanxi 041004, China*

[3]*ICQD, Hefei National Laboratory for Physical Sciences at Microscale, and Synergetic Innovation Center of Quantum Information and Quantum Physics, CAS Key Laboratory of Strongly-Coupled Quantum Matter Physics, and Department of Physics, University of Science and Technology of China, Hefei, Anhui 230026, China*

[4]*College of Physics and Energy, Shenzhen University, Shenzhen 518060, China*

(Received 16 November 2018; revised manuscript received 4 May 2019; published 22 May 2019)

Spin-orbit coupling in graphene is able to induce various topological phases and is also crucial for potential application in graphene-based spintronics. However, graphene itself exhibits extremely weak spin-orbit coupling, and it is rather challenging to enhance the spin-orbit coupling without drastically affecting its fundamental physical property in graphene via external means. In this paper, we show that the charge-compensated *n-p* codoping approach not only can overcome the main shortcomings arising from single-element adsorption in graphene but can also result in a large Rashba spin-orbit splitting. As an example, we codope heavy adatoms with outer-shell *p* electrons (e.g., Tl atoms acting as *n*-type dopants) on *p*-type doped graphene (e.g., by substituting carbon atoms with B atoms). We find the following: (1) Electrostatic attraction between *n*- and *p*-type dopants effectively enhances the adsorption and diffusion barrier of metallic adatoms and suppresses the undesirable formation of clustering. (2) Large Rashba spin-orbit splitting (∼130 meV for 6.25% B-Tl-codoped graphene) is produced due to the electrostatic interaction. (3) The charge-compensated nature and mutual screening of *n-p* codopants preserve the Dirac dispersion of charge carriers to some extent.

DOI: 10.1103/PhysRevB.99.195439

I. INTRODUCTION

Spin-orbit coupling (SOC) is a crucial ingredient in designing spintronics devices due to its advantage for spin manipulation without requiring the application of external magnetic fields [1–4]. Recent years have witnessed the great leap of exploring two-dimensional materials, in which graphene is still one of the most attractive ones because of its extremely high mobility and industrial fabrication. Ever since its first discovery in 2004, graphene has been considered a promising candidate material for future spintronics [5–7]. However, the intrinsic SOC in graphene is unrealistically weak for actual manipulation of electron spin [8]. This makes the exploration of enhancing SOC significant via external means. So far, various strategies have been proposed theoretically [9–12] and performed experimentally [13–18]. However, it has been shown to be extremely difficult to increase the extrinsic SOC without dramatically affecting other fundamental aspects of graphene's electronic structure or the material quality, e.g., preserving the remarkable properties of graphene, in particular its conelike dispersion near the Fermi level [6,12–18].

It was theoretically reported that graphene-based topological insulators with large band gaps can be realized by adsorbing *p*-shell adatoms (e.g., In and Tl) on graphene [11,19–21]. Nevertheless, in sharp contrast to these theoretical predications, in experiments it was confirmed that there is no obvious evidence of SOC or the nonlocal spin-Hall effect being observed in the proposed material systems [22]. This may arise from the weak coupling between adatoms and graphene, which may lead to the clustering formation of adatoms [22]. The dominant long-range Coulomb potential of ionized adatoms drive electrons to be spatially farther away to decrease the chance of experiencing SOC near adatoms [22]. In addition, Santos *et al.* found that new terms of the adatom-adsorption model Hamiltonian give rise to intervalley scattering, suppressing the quantum spin Hall phase. They also found that the quantum spin Hall phase cannot occur for a truly disordered system at a very low concentration of adatoms on graphene [23]. Recently, studies have confirmed that the *n-p* codoping approach using B [24], NO_2 [25], or 2,3,5,6-Tetrafluoro-7,7,8,8-tetracyanoquinodimethane (F_4-TCNQ)[26] as *p*-type codopants can greatly enhance the adsorption of metal adatoms on top of graphene, and the charge-compensated nature and mutual screening between the *n-p* codopants [27] help preserve the Dirac nature of charge carriers and the electronic performance, thereby preserving the unique linear dispersion of the charge carriers to some extent. Such a scheme was also applied to realize the high-temperature quantum anomalous Hall effect in a *n-p*-codoped topological insulator and graphene [28–30].

Inspired by this charge-compensated *n-p* codoping scheme, in this paper we study the electronic and spintronic properties of the B-Tl- and B-In-codoped graphene by using first-principles calculation methods. We first show that the electrostatic attraction between the *n*- and *p*-type dopants effectively enhances the adsorption of the metal adatoms and

*Corresponding author: hanyulei@mail.ustc.edu.cn
†Corresponding author: xuxh@dns.sxnu.edu.cn
‡Corresponding author: qiao@ustc.edu.cn

suppresses their undesirable clustering. We then find that the resulting Rashba splitting energy of the π band, from the strong electrostatic interaction between n-type Tl and p-type B, can reach about 130 meV. Furthermore, our calculation confirms that the compensated nature of n-p codoping helps to preserve the Dirac nature of charge carriers to some extent. Our finding paves the way for exploring the graphene-based spintronics without dramatically destroying the extraordinary property from the linear Dirac dispersion.

II. COMPUTATIONAL METHODS

Our first-principles calculations were performed using the projected augmented-wave method [31] as implemented in the Vienna Ab initio Simulation Package (VASP) [32–34]. The generalized gradient approximation exchange-correlation functional was adopted [35,36]. In our calculations, the lattice constant of graphene was chosen to be $a_0 = 2.46$ Å; 4×4 and 7×7 graphene supercells were considered. A vacuum buffer space over 20 Å was considered to prevent interaction between adjacent slabs. During structural relaxation, all atoms were allowed to relax along any direction, and Hellmann-Feynman forces were converged to be less than 0.01 eV/Å. For the 4×4 (7×7) graphene supercell, the kinetic energy cutoff of the plane waves was set to be 500 eV (400 eV), with the first Brillouin-zone integration being carried out using a 15×15 (5×5) Γ-centered k-point grid. The adsorption energy of the Tl/In adatoms on top of a B-doped graphene sheet was estimated using the following formula:

$$E_{\mathrm{ad}} = E_{\mathrm{Tl/In}} + E_{\mathrm{Gra+B}} - E_{\mathrm{Tot}}, \quad (1)$$

where E_{Tot}, $E_{\mathrm{Tl/In}}$, and $E_{\mathrm{Gra+B}}$ are, respectively, the energies of the B-Tl(In)-codoped graphene, Tl/In atom, and B-doped graphene systems. In our calculation, we consider that the mostly likely diffusion pathway is between the two stablest H sites with the high-symmetry site related to the next stable adsorption B site. Thus, the diffusion barrier is the energy difference between two sites [37].

III. RESULTS AND DISCUSSION

We start by studying the adsorption of Tl and In adatoms on top of graphene. Due to the hexagonal structure of graphene, there are three high-symmetry possible adsorption sites: top (on top of carbon atoms), bridge (on top of the C-C bond center), and hollow (on top of the hexagonal center). Both our calculation and previous studies confirm that the hollow sites [denoted as H_1 and H_2 in Figs. 1(a) and 1(b)] are energetically favorable for Tl and In adatoms [11]. As shown in Fig. 1(c), the adsorption energies are 0.70 and 0.69 eV for Tl and In adatoms, respectively, in agreement with previous results [11]. The relatively weak binding between these adatoms and graphene, as well as the small diffusion barriers [37,38], can lead to fast adatom migration and clustering, agreeing with the experimental observation for In-adsorbed graphene [22]. Below, we show that codoping with B will effectively suppress these undesirable effects. When doped in graphene by substituting a C atom, the B atom becomes a p-type dopant and contributes a hole to the graphene Fermi sea. It has been shown that doping B leads to negligible variance in the

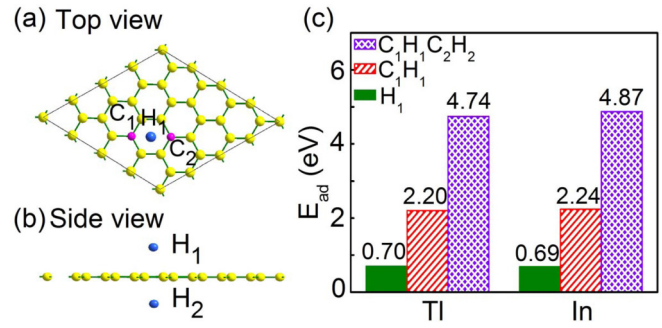

FIG. 1. (a) Top view and (b) side view of B-Tl(In)-codoped graphene. $H_{1,2}$ represent the hollow sites of the top and bottom sides for Tl/In adsorption; $C_{1,2}$ represent the positions of B substitution. Blue, pink, and yellow indicate Tl (In), B, and C atoms, respectively. (c) Adsorption energies of Tl/In adatoms on top of pristine graphene (olive), B-Tl(In)-codoped graphene (red), and two pairs of B-Tl(In)-codoped graphene (violet).

unique electronic properties of graphene aside from providing extra holes [39–41]. Since both Tl and In adatoms are n-type dopants in graphene [11], they exhibit opposite charge states compared with B dopants. Therefore, one can expect that the electrostatic attraction between Tl/In adatoms and B dopants is able to stabilize the diluted adsorption of the metal adatoms.

To show this is indeed the case, we calculated the adsorption energies of Tl and In adatoms by codoping with B atoms in the stablest configuration of C_1H_1 (one Tl/In atom sitting at the H_1 position and one B atom substituting one carbon atom at the C_1 position) as displayed in Fig. 1(a). From Fig. 1(c), one can see that codoping B atoms results in an increase of ~1.5 eV in the adsorption energy of Tl and In adatoms, i.e., $E_{\mathrm{ad}} = 2.20$ and 2.24 eV for Tl and In, respectively. Moreover, when the codoping concentration increases [e.g., the stablest $C_1H_1C_2H_2$ configuration in Fig. 1(a)], the adsorption energies of Tl and In adatoms increase to 4.74 and 4.87 eV, indicating a stronger attractive interaction between Tl/In and B adatoms. Such a strong attraction plays a crucial role in stabilizing Tl/In adatoms at positions close to substitutive boron codopants, effectively suppressing the migration and clustering of the metal adatoms on graphene.

In addition to adsorption energy, the diffusion barrier is another important parameter to understand the adsorption stability of the metal adatoms on the material surface. In general, the diffusion barrier is obtained by the energy difference between the H site and B site because the two sites are the stablest adsorption sites for Tl and In adatoms on graphene. As displayed in Fig. 2, the diffusion barriers of Tl and In adatoms on B-doped graphene become increased compared with those of Tl and In on graphene. For example, the diffusion barrier of In (Tl) adatoms is increased from 1.55 (0.32) eV on the surface of graphene to 1.71 (0.58) eV on the surface of B-doped graphene. It is worth noting that the diffusion barrier of Tl on B-doped graphene is 0.58 eV, which is larger than 0.50 eV. The latter corresponds roughly to the threshold energy of atomic migration at room temperature. In a previous study [42], the authors found that the p-type charge doping can increase the adsorption energy and diffusion barrier of a metal element such as Fe adatoms on graphene. That is in agreement with our result that B doping (p-type doping)

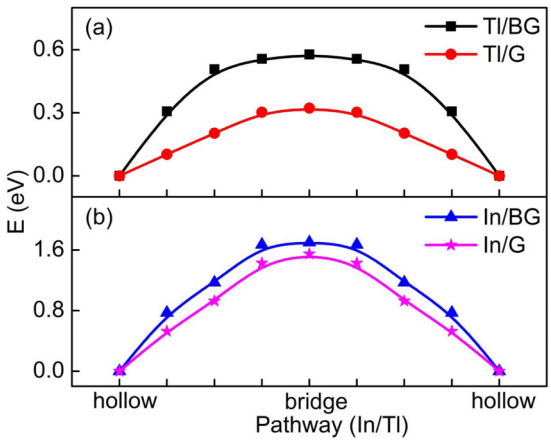

FIG. 2. Diffusion barriers of (a) Tl and (b) In adatoms on B-doped graphene (BG) and graphene (G).

can enhance the adsorption of Tl and In adatoms on graphene. In fact, the stability of metal adatoms on graphene in experiments is found to be in agreement with theoretical estimation via the evaluation of the binding energy and diffusion barrier. For example, in a study of the metal-atom interaction on graphene, Hupalo *et al.* found the correlation between the experimental measured diffusion length with binding energy and the diffusion barrier of metal adatoms on graphene [43]. Therefore, it is reasonable to conclude that the adsorption energies and diffusion barriers of Tl and In adatoms on B-doped graphene can better reflect their stability.

We now move to the spin splitting of the B-Tl-codoped graphene. In Fig. 3(a), we display the band structure of Tl-adsorbed graphene by invoking the SOC. One can see that it opens up a tiny band gap (26 meV) to host the well-known quantum spin-Hall effect due to the enhancement of intrinsic SOC [11]. It is noteworthy that the Fermi level deviates about 0.80 eV from the neutral Dirac point. When B atoms are codoped in the specific C_1H_1 configuration, in Fig. 3(b) without SOC, one can find that the Fermi level is tailored close to the Dirac point due to the one-by-one charge compensation. The *n*-*p* codoping approach proposed in the present study actually offers convenient tunability of the Fermi level, e.g., by manipulating the ratio between *n*- and *p*-type dopants. Another finding is that a much larger band gap (110 meV) opens at Dirac points due to the inversion symmetry breaking from the imbalanced sublattice potential that arises from the B substitution. When the SOC is further invoked, one can see that obvious band splitting exists by comparing the bands from Figs. 3(b) and 3(c). In addition, we can also find that the band gaps at the Dirac points become small for B-Tl (from 110 to 60 meV) and B-In (from 112 to 102 meV) codoped graphene when spin-orbit coupling is considered. As shown in Figs. 3(d) and 3(i), this decrease in band gaps arises mainly

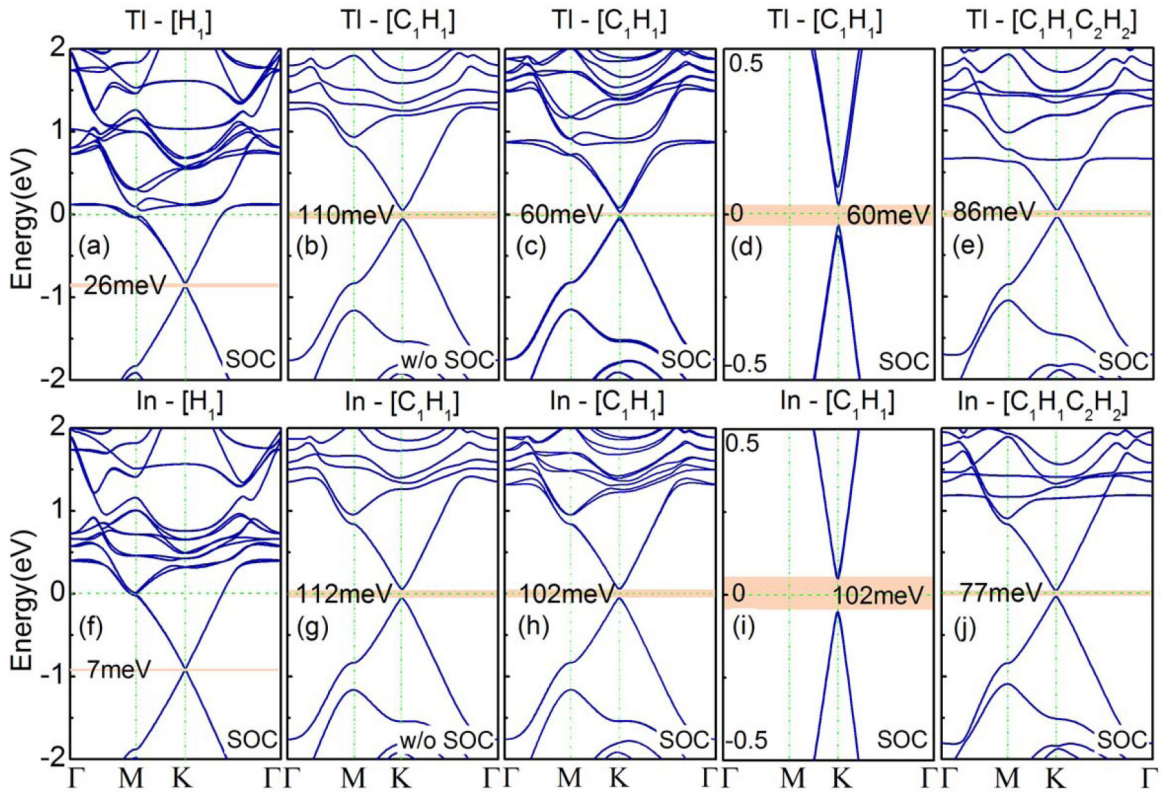

FIG. 3. Band structures along high-symmetry lines of graphene with various adatoms: (a) One Tl adatom at the H_1 position with SOC. (b)–(d) One pair of B-Tl adatoms at the C_1 and H_1 positions (b) without and (c) with SOC and (d) a close-up view of the band structure with SOC near the Fermi level. (e) Two pairs of B-Tl adatoms at the $C_{1,2}$ and $H_{1,2}$ positions with SOC. (f) One In adatom at the H_1 position with SOC. (g)–(i) One pair of B-In adatoms at the C_1 and H_1 positions (g) without and (h) with SOC and (i) a close-up view of the band structure with SOC near the Fermi level. (j) Two pairs of B-In adatoms at the $C_{1,2}$ and $H_{1,2}$ positions with SOC. The corresponding values of band gaps are also provided by shaded areas.

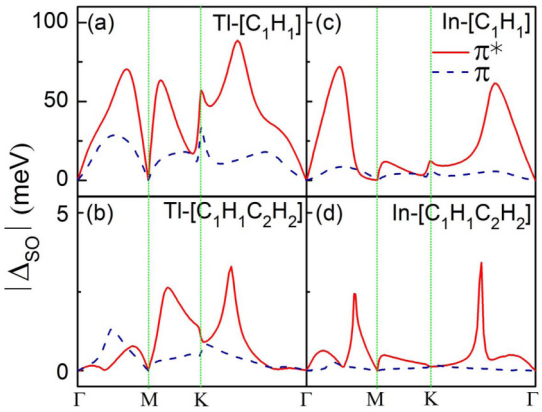

FIG. 4. The absolute values of SOC Δ_{SO} for the π (blue dashed lines) and π^* (red solid lines) bands along Γ-M-K-Γ high-symmetry lines in graphene systems with (a) one pair of B-Tl codopants, (b) one pair of B-In codopants, (c) two pairs of B-Tl codopants, and (d) two pairs of B-In codopants.

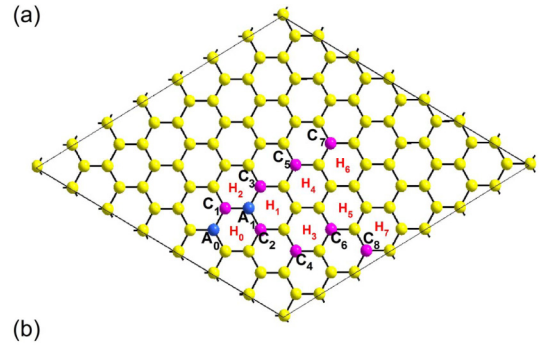

Conf.	$[C_1H_2]$	$[C_2H_1]$	$[A_1H_1]$	$[A_1H_2]$
E_{rel} (eV)	0	-1.014	-0.809	-0.886

FIG. 5. (a) A 7×7 graphene supercell. H_0–H_7 represent the hollow sites for Tl adsorption, while A_0–A_1 (light blue balls) and C_1–C_8 (pink balls) represent the positions of B substitution of different sublattices of graphene. (b) The relative stability of four configurations with two pairs of B-Tl-codoped graphene. One pair is fixed at A_0H_0, and the other moves from A_1H_0 to C_8H_7.

from the spin splitting in the corresponding valence band maximum and conduction band minimum. Larger spin splitting occurs in the B-Tl-codoped graphene but not in B-In-codoped graphene, leading to a more obvious decrease of band gap in the B-Tl-codoped graphene.

In graphene, there are usually two kinds of representative SOCs, i.e., intrinsic SOC and extrinsic Rashba SOC. For the single Tl adsorption, the resulting weak intrinsic SOC dominates, leading to the quantum spin-Hall effect. However, for the B-Tl-codoped system, it clearly seems that the spin splitting is stronger than that in Tl-doped case. Thus, we assume that the codoping mechanism greatly increases the Rashba SOC. In order to verify this assumption, we consider the adsorption configuration of $C_1H_1C_2H_2$ with two pairs of B-Tl codopants. In such a consideration, the two Tl atoms are almost symmetrically distributed across the graphene plane, which recovers mirror symmetry to eliminate the Rashba SOC. One needs to notice that although the two B atoms substitute the carbon atoms at different sublattices, the influence from two Tl atoms makes it unbalanced at sublattice potentials; thus, a small band gap (86 meV) still exists at the Dirac point. Most importantly, a remarkable observation is that the bands become doubly degenerate, strongly indicating the vanishing of Rashba SOC. The above analysis shows that codoping B-Tl in graphene can increase the extrinsic Rashba SOC when the Tl atoms are adsorbed on only one side of graphene, which can easily be realized in experiment.

As shown in Figs. 3(f) to 3(j), the B-In-codoped graphene exhibits characteristics similar to those in B-Tl-codoped graphene, e.g., the adsorption stability, band structure, and spin-splitting. In Fig. 4, we display the k dependence of spin splitting Δ_{SO} of the π and π^* bands along the high-symmetry lines, which are highly relevant to the transport properties because they are present near the Fermi level. One can find that in B-Tl-codoped graphene the maximum spin-splitting strengths for the π and π^* bands are, respectively, about 50 and 90 meV at the C_1H_1 configuration, while the values are, respectively, 10 and 75 meV for the B-In-codoped graphene. As discussed above, at the $C_1H_1C_2H_2$ configuration the inversion symmetry is recovered; therefore, the spin splitting Δ_{SO} for either the π or π^* band becomes weaker than 4 meV. These results suggest that the large spin splitting is mainly contributed by the Rashba spin-orbit coupling. Importantly, the linear dispersion of graphene is well preserved after the n-p codoping (see Fig. 3).

There are various possible codoping configurations in experiment. Below, we first study the influence of codoping configurations on Rashba spin splitting by taking the B-Tl-codoped graphene as an example. Figure 5(a) displays the schematic illustration of B-Tl-codoped graphene. We consider two B-Tl pairs in a 7×7 graphene supercell. One Tl atom is placed at H_0, paired with a B atom at site A_0, and the other Tl atom is assumed to move from the H_1 to H_7 site with its codoping partnered B atoms always substituting the nearest-neighbor carbon site. In order to represent these configurations concisely, in each square bracket we label only the positions of the second B and second Tl adatoms. For example, $[C_1H_2]$ corresponds to the $A_0H_0C_1H_2$ configuration. Figure 5(b) displays the relative energy for some typical configurations with the reference energy of $[C_1H_2]$ being zero. One can see that the further C-site doping of B atoms is stabler in the B-Tl-codoped graphene. Thus, most configurations designed in our study are C-site B substitution, with some of them distributing along the zigzag direction [C_1, C_3, C_5, and C_7 in Fig. 4(a)] and others residing along the armchair direction [C_2, C_4, C_6, and C_8 in Fig. 4(a)]. Figure 6 summarizes the relative energies of all designed configurations and the corresponding spin splitting for the π and π^* bands between the Γ and M points. From Fig. 6, one finds that the $[C_2H_1]$ configuration is the stablest one with a spin splitting of about 50 meV for the π^* band. In addition, one can also see that the configuration has a negligible influence on spin splitting of graphene when the distance of two B-Tl pairs becomes even longer.

Now, we move to explore the dependence of the spin splitting on the codoping concentration of B-Tl in graphene. Figure 7 displays the band structures and corresponding spin-splitting [Figs. 7(b), 7(d), 7(f), and 7(h)] for different

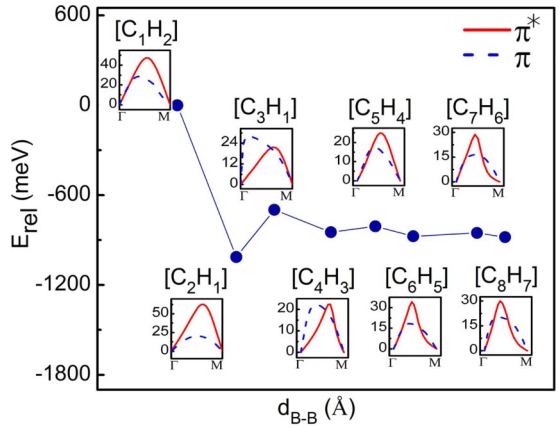

FIG. 6. The relative stability vs pair separation distance in the graphene supercell with two pairs of B-Tl codopants. The insets are the absolute values of spin-orbit splitting for the π (blue dashed line) and π^* (red solid line) bands along the Γ and M points.

B-Tl codoping concentrations (i.e.,1.56%, 2.04%, 4.00%, and 6.25%) at the stablest $[C_2H_1]$ configuration. From Figs. 7(a) to 7(g), one can find that the spin splitting becomes larger with the increase of codoping concentration [see details of spin splitting in Figs. 7(b) to 7(h)]. For example, the spin splitting in our *n-p*-codoped graphene can reach 130 meV at 6.25% B/Tl-codoped concentration, which is much larger than the typical Rashba spin splitting in the conventional III-V an II-VI semiconductor quantum wells (e.g., < 30 meV) [44,45]. Certainly, the spin splitting in our *n-p*-codoped graphene is also smaller than those observed in the Au surface state (140 meV) [46,47] and Bi(111) surface state (200 meV) [48]. Furthermore, it is comparable to the enhanced surface Rashba splitting (of several hundred meV) in various graphene/substrate systems [14,15,18]. And our scheme not only can produce a large Rashba spin splitting but can also perfectly preserve the desired electronic structure of graphene, which implies great practical application in designing graphene-based spintronics.

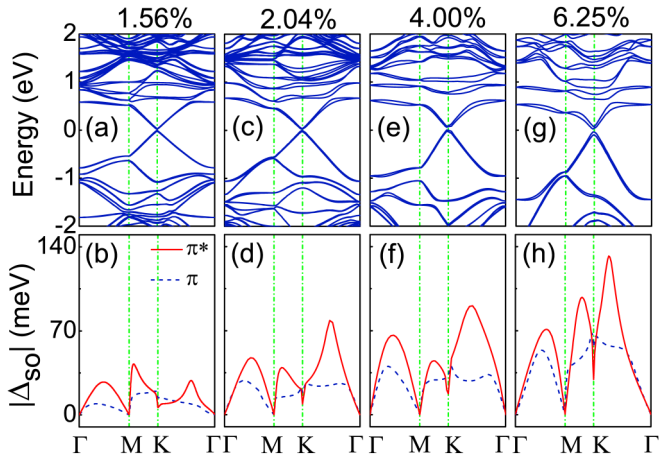

FIG. 7. (a), (c), (e), and (g) Band structures and (b), (d), (f), and (h) corresponding absolute values of spin-orbit splitting Δ_{SO} for the π (blue dashed line) and π^* (red solid line) bands along high-symmetry lines in the 1.56%, 2.04%, 4.00%, and 6.25% B-Tl-codoped graphene.

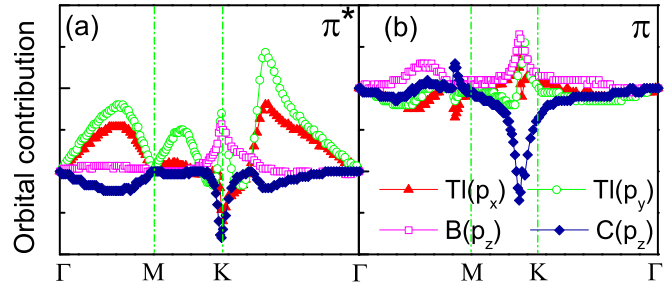

FIG. 8. The orbitally resolved contributions (in arbitrary units) of Tl, B, and carbon for the (a) π^* and (b) π bands in the 6.25% B-Tl-codoped graphene. The solid triangles and rhombuses represent the data for p_x orbitals of Tl atoms and p_z orbitals of C atoms, respectively. The open circles and squares represent the data for p_y orbitals of Tl atoms and p_z orbitals of B atoms, respectively.

To gain further insight into the spin splitting, we study the orbitally resolved contribution from different atoms to the π and π^* bands at the 6.25% B-Tl codoping concentration. For the spin splitting of the π^* band [see solid line in Fig. 7(h)], the orbitally resolved contributions from Tl, B, and C atoms are displayed in Fig. 8(a). One can see that three peaks of Δ_{SO} in Fig. 7(h) correspond to the contribution of $p_{x,y}$ orbitals of Tl atoms along the high-symmetry lines. At the K point, the sharp decrease of Δ_{SO} is attributed to the strong hybridization among orbitals from B, carbon, and Tl atoms. For the spin splitting of the π band [see dashed line in Fig. 7(h)], the hybridization among B, carbon, and Tl atoms also plays an important role in the presence of Δ_{SO}, as displayed in Fig. 8(b). Therefore, the above analysis indicates that the interactions of B and carbon π states with p states of Tl are the origin of the giant Rashba spin splitting in *n-p*-codoped graphene. It is noteworthy that the large Rashba spin-orbit splitting in B-Re- and B-Pt-codoped graphene can also be introduced [30]. But the spin-orbit splitting in B-Re- and B-Pt-codoped graphene mainly originates from the 5d orbital [30]. We know that the d orbitals are usually more localized than p orbitals, which can be reflected by the band structures near the Fermi level in B-Tl- and B-Pt-codoped graphene. Thus, we find that the effective mass of an electron or hole in B-Tl-codoped graphene is smaller than that in B-Pt-codoped graphene. In addition, the Fermi level is located in the gap of the B-Tl-codoped graphene but in the valence band of the B-Pt-codoped graphene. This is because that p electron is much freer than the d electron. This difference reflects the fact that the charge is completely compensated in the B-Tl-codoped graphene but not compensated in the B-Pt-codoped graphene. So the charge scattering in the B-Tl-codoped graphene is weaker than that in the B-Pt-codoped graphene. The smaller effective mass of the carrier and weaker charge scattering in the B-Tl-codoped graphene are beneficial to the carrier mobility. As reported, it is extremely difficult to increase the extrinsic spin-orbit coupling without dramatically affecting other fundamental aspects of its electronic structure or the material quality, e.g., preserving the remarkable properties of graphene, in particular its conelike dispersion near the Fermi level. Strikingly, in this work we are able to introduce large Rashba spin-orbit splitting and preserve the desired electronic

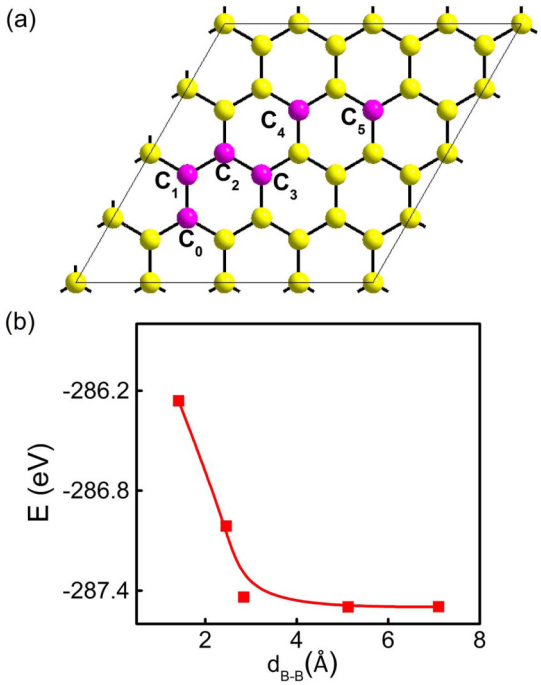

FIG. 9. (a) A 4×4 supercell of a graphene single layer. C_0–C_5 represent the possible positions of B substitution. One B is fixed at C_0, and the other moves from C_1 to C_5. (b) The total energies of different configurations of B-doped graphene vs B-B separation.

structure of graphene to some extent. The underlying reason is that interaction between the graphene π state and Tl p state is the physical origin of giant spin-orbit splitting in B-Tl-codoped graphene.

We close by commenting on the possible experimental realization of B-Tl-codoped graphene. In experiment, two steps are needed to produce the B-Tl(In)-codoped graphene. The first step is to realize the B-doped graphene. In our study, we designed five configurations with different B-B distances [see Fig. 9(a)] and obtained their relative stability energies [Fig. 9(b)]. One can find that the configuration with larger B-B separation in B-doped graphene is the stablest one, indicating that the interaction between substituted B atoms is repulsive. Therefore, B substitution in graphene should be random, and the B domain is not easy to form in B-doped graphene at small or moderate doping concentrations. This finding is in good agreement with many experimental observations on B-doped graphene [41,49–51]. Based on our results and previous experimental findings, B-doped graphene with a random substitution manner is easy to realize in experiment. The second step is to assemble the Tl or In adatoms on the surface of B-doped graphene. It is known that metal adatoms (such as Co, Fe, and In) have been successfully assembled on the surface of graphene in experiments. For example, Brar *et al.* prepared Co adatoms on graphene by *e*-beam evaporation and found that the electronic structure of Co adatoms can be tuned by applying gate voltage and that the Co atoms can be reversibly ionized [52]; Jia *et al.* realized In adatoms on graphene by thermal deposition and carried out the transport measurements [22]. Thus, Tl or In adatoms can be adsorbed around the substituted B atoms in B-doped graphene at small doping concentration due to the strong "pinning" effect of B dopants to Tl or In adatoms. At this point, diluted B/Tl(In)-codoped graphene can be formed in experiment. The *n*-*p* codoping approach established here provides a viable route to introduce strong extrinsic Rashba spin-orbit coupling without destroying much of the unique linear dispersion of graphene and may stimulate additional efforts in the further exploration of graphene based spintronics.

IV. CONCLUSION

In summary, by using density functional theory calculations, we proposed a scheme based on *n*-*p* codoping that can effectively result in large Rashba spin-orbit coupling in graphene while keeping its unique linear dispersion to some extent. We proposed to codope the metal atoms (e.g., Tl and In) with outer-shell p electrons into the B-substituted graphene. We showed that the electrostatic attraction between *n*- and *p*-type codopants can effectively enhance the adsorption and diffusion barrier of the metal adatoms and suppress the possible undesirable clustering. We then found that the calculated Rashba spin splitting of B/Tl-codoped graphene can reach about 130 meV, which is several orders of magnitude higher than the reported intrinsic spin-orbit coupling. Further analysis showed that the strong interaction between *n*-type Tl and *p*-type B and carbon π states plays an important role in inducing giant Rashba-type spin-orbit coupling. Our finding sheds some light on designing larger spin-orbit coupling in graphene and further on producing graphene-based spintronics.

ACKNOWLEDGMENTS

This work was financially supported by the National Key R&D Program (Grant No. 2016YFA0301700), NNSFC (Grants No. 11104173, No. 61434002, No. 51025101, No. 11504240, and No. 11474265), and the China Government Youth 1000-Plan Talent Program. The Supercomputing Center of USTC is gratefully acknowledged for the high-performance computing assistance.

[1] A. Manchon, H. C. Koo, J. Nitta, S. M. Frolov, and R. A. Duine, Nat. Mater. **14**, 871 (2015).

[2] C. R. Ast, J. Henk, A. Ernst, L. Moreschini, M. C. Falub, D. Pacilé, P. Bruno, K. Kern, and M. Grioni, Phys. Rev. Lett. **98**, 186807 (2007).

[3] G. Bihlmayer, S. Blügel, and E. V. Chulkov, Phys. Rev. B **75**, 195414 (2007).

[4] H. Mirhosseini, I. V. Maznichenko, S. Abdelouahed, S. Ostanin, A. Ernst, I. Mertig, and J. Henk, Phys. Rev. B **81**, 073406 (2010).

[5] A. K. Geim and K. S. Novoselov, Nat. Mater. **6**, 183 (2007).
[6] W. Han, R. K. Kawakami, M. Gmitra, and J. Fabian, Nat. Nanotechnol. **9**, 794 (2014).
[7] C. L. Kane and E. J. Mele, Phys. Rev. Lett. **95**, 146802 (2005).
[8] Y. Yao, F. Ye, X.-L. Qi, S.-C. Zhang, and Z. Fang, Phys. Rev. B **75**, 041401(R) (2007).
[9] A. H. Castro Neto and F. Guinea, Phys. Rev. Lett. **103**, 026804 (2009).
[10] Z. Qiao, S. A. Yang, W. Feng, W.-K. Tse, J. Ding, Y. Yao, J. Wang, and Q. Niu, Phys. Rev. B **82**, 161414(R) (2012).
[11] C. Weeks, J. Hu, J. Alicea, M. Franz, and R. Wu, Phys. Rev. X **1**, 021001 (2011).
[12] D. Ma, Z. Li, and Z. Yang, Carbon **50**, 297 (2012).
[13] J. Balakrishnan, G. K. W. Koon, M. Jaiswal, A. H. Castro Neto, and B. Ozyilmaz, Nat. Phys. **9**, 284 (2013).
[14] D. Marchenko, A. Varykhalov, M. R. Scholz, G. Bihlmayer, E. I. Rashba, A. Rybkin, A. M. Shikin, and O. Rader, Nat. Commun. **3**, 1232 (2012).
[15] A. Avsar, J. Y. Tan, T. Taychatanapat, J. Balakrishnan, G. K. W. Koon, Y. Yeo, J. Lahiri, A. Carvalho, A. S. Rodin, E. C. T. O'Farrell, G. Eda, A. H. Castro Neto, and B. Ozyilmaz, Nat. Commun. **5**, 4875 (2014).
[16] A. Varykhalov, J. Sánchez-Barriga, A. M. Shikin, C. Biswas, E. Vescovo, A. Rybkin, D. Marchenko, and O. Rader, Phys. Rev. Lett. **101**, 157601 (2008).
[17] Y. S. Dedkov, M. Fonin, U. Rudiger, and C. Laubschat, Phys. Rev. Lett. **100**, 107602 (2008).
[18] Z. Wang, D. Ki, H. Chen, H. Berger, A. H. MacDonald, and A. F. Morpurgo, Nat. Commun. **6**, 8339 (2015).
[19] H. Jiang, Z. Qiao, H. Liu, J. Shi, and Q. Niu, Phys. Rev. Lett. **109**, 116803 (2012).
[20] O. Shevtsov, P. Carmier, C. Groth, X. Waintal, and D. Carpentier, Phys. Rev. B **85**, 245441 (2012).
[21] Y. Ren, Z. Qiao, and Q. Niu, Rep. Prog. Phys. **79**, 066501 (2016).
[22] Z. Jia, B. Yan, J. Niu, Q. Han, R. Zhu, D. Yu, and X. Wu, Phys. Rev. B **91**, 085411 (2015).
[23] F. J. dos Santos, D. A. Bahamon, R. B. Muniz, K. McKenna, E. V. Castro, J. Lischner, and A. Ferreira, Phys. Rev. B **98**, 081407(R) (2018).
[24] S. Qi, H. Chen, X. Xu, and Z. Zhang, Carbon **61**, 609 (2013).
[25] R. Zhang, Y. Luo, S. Qi, and X. Xu, Appl. Surf. Sci. **305**, 768 (2014).
[26] X. Zhang, S. Qi, and X. Xu, Carbon **95**, 65 (2015).
[27] W. Zhu, Z. Zhang, and E. Kaxiras, Phys. Rev. Lett. **100**, 027205 (2008).
[28] S. Qi, Z. Qiao, X. Deng, E. D. Cubuk, H. Chen, W. Zhu, E. Kaxiras, S. B. Zhang, X. Xu, and Z. Zhang, Phys. Rev. Lett. **117**, 056804 (2016).
[29] X. Deng, S. Qi, Y. Han, K. Zhang, X. Xu, and Z. Qiao, Phys. Rev. B **95**, 121410(R) (2017).
[30] X. Deng, H. Yang, S. Qi, X. Xu, and Z. Qiao, Front. Phys. **13**, 137308 (2018).
[31] P. E. Blöchl, Phys. Rev. B **50**, 17953 (1994).
[32] G. Kresse and J. Hafner, Phys. Rev. B **49**, 14251 (1994).
[33] G. Kresse and J. Hafner, Phys. Rev. B **47**, 558 (1993).
[34] G. Kresse and J. Furthmüller, Comput. Mater. Sci. **6**, 15 (1996).
[35] J. P. Perdew, K. Burke, and M. Ernzerhof, Phys. Rev. Lett. **77**, 3865 (1996).
[36] J. P. Perdew, K. Burke, and M. Ernzerhof, Phys. Rev. Lett. **78**, 1396 (1997).
[37] K. T. Chan, J. B. Neaton, and M. L. Cohen, Phys. Rev. B **77**, 235430 (2008).
[38] H. Johll, H. C. Kang, and E. S. Tok, Phys. Rev. B **79**, 245416 (2009).
[39] A. Lherbier, X. Blase, Y. M. Niquet, F. Triozon, and S. Roche, Phys. Rev. Lett. **101**, 036808 (2008).
[40] T. B. Martins, R. H. Miwa, A. J. R. da Silva, and A. Fazzio, Phys. Rev. Lett. **98**, 196803 (2007).
[41] Y. Tang, L. Yin, Y. Yang, X. Bo, Y. Cao, H. Wang, W. Zhang, I. Bello, S. Lee, H. Cheng, and C. Lee, ACS Nano **6**, 1970 (2012).
[42] W. Ming and F. Liu, Appl. Phys. Lett. **105**, 071609 (2014).
[43] M. Hupalo, X. Liu, C. Wang, W. Lu, Y. Yao, K. Ho, and M. C. Tringides, Adv. Mater. **23**, 2082 (2011).
[44] Y. S. Gui, C. R. Becker, N. Dai, J. Liu, Z. J. Qiu, E. G. Novik, M. Schafer, X. Z. Shu, J. H. Chu, H. Buhmann, and L. W. Molenkamp, Phys. Rev. B **70**, 115328 (2004).
[45] J. Nitta, T. Akazaki, H. Takayanagi, and T. Enoki, Phys. Rev. Lett. **78**, 1335 (1997).
[46] H. Ishida, Phys. Rev. B **98**, 205412 (2018).
[47] S. LaShell, B. A. McDougall, and E. Jensen, Phys. Rev. Lett. **77**, 3419 (1996).
[48] Yu. M. Koroteev, G. Bihlmayer, J. E. Gayone, E. V. Chulkov, S. Blugel, P. M. Echenique, and Ph. Hofmann, Phys. Rev. Lett. **93**, 046403 (2004).
[49] P. Marconcini, A. Cresti, F. Triozon, G. Fiori, B. Biel, Y. Niquet, M. Macucci, and S. Rochez, ACS Nano **6**, 7942 (2012).
[50] L. Zhao, M. Levendorf, S. Goncher, T. Schiros, L. Palova, A. Zabet-Khosousi, K. T. Rim, C. Gutierrez, D. Nordlund, C. Jaye, M. Hybertsen, D. Reichman, G. W. Flynn, J. Park, and A. N. Pasupathy, Nano Lett. **13**, 4659 (2013).
[51] H. Wang, Y. Zhou, D. Wu, L. Liao, S. Zhao, H. Peng, and Z. Liu, Small **9**, 1316 (2013).
[52] V. M. Brar, R. Decker, H. M. Solowan, Y. Wang, L. Maserati, K. T. Chan, H. Lee, C. O. Girit, A. Zettl, S. G. Louie, M. L. Cohen, and M. F. Crommie, Nat. Phys. **7**, 43 (2011).